

# Redshift estimation from low-resolution prism SEDs with an NGST MOS

Harry I. Teplitz<sup>1,2</sup>,

Eliot Malumuth<sup>1,3</sup>, Bruce E. Woodgate<sup>1</sup>, S. Harvey Moseley<sup>4</sup>, Jonathan P. Gardner<sup>1</sup>,  
Randy A. Kimble<sup>1</sup>, Charles W. Bowers<sup>1</sup>, Alexander S. Kutyrav<sup>3,4,5</sup>, Rainer K. Fettig<sup>3,6</sup>,  
Richard P. Wesenberg<sup>7</sup>, John E. Mentzell<sup>8</sup>

Goddard Space Flight Center, Greenbelt MD 20771

Electronic mail: hit@binary.gsfc.nasa.gov

Received \_\_\_\_\_; accepted \_\_\_\_\_

---

<sup>1</sup>Laboratory for Astronomy and Solar Physics, Code 681

<sup>2</sup>NOAO Research Associate

<sup>3</sup>Raytheon ITSS Corp., Lanham, MD 20706

<sup>4</sup>Laboratory for Astronomy and Solar Physics, Code 685

<sup>5</sup>Sternberg Astronomical Institute, Moscow

<sup>6</sup>Laboratory for Extraterrestrial Physics, Code 693

<sup>7</sup>Systems, Technology, And Advanced Concepts (STAAC), Code 730

<sup>8</sup>Instrument Technology Center, Code 551

## ABSTRACT

We discuss the utility of a low resolution prism as a component of a Multi-Object Spectrometer for NASA’s proposed Next Generation Space Telescope (NGST). Low resolution prism spectroscopy permits simultaneous observation of the  $0.6 - 5\mu\text{m}$  wavelength regime at  $R \lesssim 50$ . Such data can take advantage of the modern techniques in spectral energy distribution (SED) fitting to determine source redshifts, sometimes called “photometric redshifts”. We compare simulated prism observations with filter imaging for this purpose with NGST.

Low resolution prism observations of galaxy SED’s provide a significant advantage over multi-filter observations for any realistic observing strategy. For an ideal prism in sky background limited observing, the prism has a signal-to-noise advantage of square root of the resolution over serial observations by filters with similar spatial and spectral resolution in equal integration time. For a realistic case the advantage is slightly less and we have performed extensive simulations to quantify it. We define strict criteria for the recovery of input redshifts, such that to be considered a success redshift residuals must be  $\delta_z < 0.03 + 0.1 \times \log z$ . The simulations suggest that in  $10^5$  seconds a realistic prism will recover (by our definition of success) the redshift of  $\sim 70\%$  of measured objects (subject to MOS selection) at  $K_{AB} < 32$ , compared to less than 45% of the objects with serial filter observations. The advantage of the prism is larger in the regime of faint ( $K_{AB} > 30$ ) objects at high redshift ( $z > 4$ ), where the prism recovers 80% of redshifts, while the filters recover barely 35% to similar accuracy. The primary discovery space of NGST will be at the faintest magnitudes and the highest redshifts. Many important objects will be too faint for follow up at higher spectral resolution, so prism observations are the optimal

technique to study them. Prism observations also reduce the contamination of high redshift samples by lower redshift interlopers.

*Subject headings:* Instrumentation : Spectrographs – Techniques : Spectroscopic  
– infrared : galaxies – galaxies : redshifts

## 1. Introduction

A primary science driver of the Next Generation Space Telescope mission (NGST; Stockman 1997) will be near-IR observations of the very high redshift universe ( $z > 4$ ). Low resolution ( $R < 100$ ) and medium resolution ( $R \sim 1000$ ) spectroscopy will probe the rest-frame ultra-violet (UV) of the youngest galaxies. The unprecedented light collecting power of an 8m telescope away from the glow and opacity of the Earth’s atmosphere in the IR will reveal objects that could neither be discovered nor followed-up from ground-based observatories. It will be necessary to make the most efficient use of the light gathered by NGST observations alone.

The Hubble Deep Fields (HDF-North and HDF-South, see Williams et al. 1996, 2000) have shown the tremendous power of spectral energy distribution (SED) fitting redshift estimation, “photometric” redshifts, for the study of objects either too numerous or too faint to be followed-up spectroscopically (see Connolly et al. 1997, Lanzetta et al. 1996). NGST deep fields will certainly need to utilize this technique. Traditional photometric redshifts have used serial observations in several filters with an imager to obtain the low resolution SEDs from which redshifts are inferred. We suggest the use of the common practice of objective prism spectroscopy as a more efficient means to obtain the SEDs of galaxies in deep NGST observations. These prism observations will be made through an entrance aperture mask, to prevent spectral overlap and to minimize sky background.

Prism observations have one clear advantage – their simultaneous observation of the SED at all wavelengths. Indeed, near-IR prisms are already planned for ground based instrumentation (e.g. Oliva et al. 1999). We will show that prism spectra enjoy a significant advantage over serial filter observations for the study of the faintest galaxies with NGST despite the limitations associated with an entrance mask.

NGST will need to simultaneously obtain spectra of many galaxies. The preferred

approach to this problem is a programmable multi-object spectrograph (MOS; see Mather et al. 2000); other approaches include an integral field spectrograph (IFU; Le Fevre et al. 2000) or Fourier-Transform spectrograph (FTS; Graham et al. 1998). Such a MOS could include a prism mode. Unlike optical ground-based spectrographs which can make new aperture masks or easily reposition fibers, a space borne cryogenic spectrograph will need slitmasks that can be controlled purely by software. Roberts et al. (2000) and Buckham et al. (2000) have studied mechanical MOS designs (repositioning slits of fixed size or fibers with complete software control), but the preferred solution is the use of microelectronic mechanical systems technology (MEMS). Such technology can be applied as an array of slits (transmissive or reflective) that are used as a programmable field selector. Two MEMS entrance mask designs have been studied – micro-shutters (Moseley et al. 2000) and micro-mirrors (MacKenty et al. 2000).

In this paper we explore the utility of prism spectroscopy as one of the primary modes for NGST observations of high redshift galaxies. We have carried out extensive Monte-Carlo simulations to examine the trades involved in choosing a prism as the primary “photometric redshift machine” for NGST instead of relying on the imager for this purpose. We conclude that prism observations are more successful in recovering object redshifts than serial filter observations in equal total time.

We begin by reviewing the technique of SED-fitting for estimating galaxy redshift (section 2). Next, we discuss the details of our simulations (section 3) and our primary result. We outline the assumptions we make about both the imager and the spectrograph. We then show (section 4) the effect of varying each of these assumptions in turn, to establish that our conclusion is robust given the many unknowns of an instrument that may be half a decade away. We then discuss (section 5) the advantages of a prism on different areas of NGST science. We discuss the limitation inherent in MOS observations (that not every

object in a field can be observed in a single “shot”). Finally, in section 6, we summarize our results.

## 2. SED Fitting and Photometric Redshifts

Photometric redshifts have been successfully applied to many catalogs of galaxy photometry (see Koo 1985, Brunner et al. 1997, Connolly et al. 1997, Lanzetta et al. 1996, Giallongo et al. 1998; for a review see Hogg et al. 1998). The SED of a candidate galaxy is compared to a database of template spectra at all redshifts; the best fit between the two is considered to be the photometric redshift. The idea, while simple, relies on the complicated question of choosing the proper template spectra.

Remarkably good results ( $\sigma_z/z \sim 0.05$ ) are obtained out to redshifts  $z \sim 6$  with only a handful of observed low- $z$  templates (e.g. Lanzetta et al. 1996 using the spectra of Coleman, Wu & Weedman 1980 ) or with a standard set of spectral synthesis models (e.g. Giallongo et al. 1998 using the GISSEL98 models of Bruzual & Charlot 1993 ). The errors in inferred redshift are the result of a combination of photometric uncertainty and the intrinsic difference between observed galaxies and the expected templates. In a modified technique, Brunner et al. (1997) achieved better accuracy by fitting the integrated colors of empirical spectra at the redshifts and galaxy types of interest. Ideally, this method eliminates the uncertainty resulting from inappropriate templates. The empirical-fitting method requires a large database of spectra over all redshifts, but such data would likely be available from a few deep fields observed with NGST spectroscopy. For our simulations, we have assumed that the empirical-fitting method is a viable option, and have chosen to model the recovery of redshifts using very similar input and output model templates.

Specifically, for our comparison template sets we have used a grid of 10 spectra from

the GISSSEL96 (see Bruzual & Charlot 1993) spectral synthesis models, covering 0.5-20 Gyr ages, with solar or lower metallicity and Salpeter IMF's. Figure 1 shows the comparison template spectra used for the simulations. The spectra are redshifted to 100 discrete redshifts between 0 and 15, evenly spaced in  $\sqrt{z}$ , then convolved with the filter or prism response. The input spectra for the simulations are constructed in a similar way, using slightly different ages for the GISSSEL96 models, a continuous redshift distribution, and have noise added (see Section 3.1). The simulated galaxies and comparison templates are then compared at each resolution element. Following typical photometric redshift techniques, we perform  $\chi^2$  tests on the suite of redshifted template spectra. The inferred redshift is the one with the lowest  $\chi^2$  value.

We note that  $\chi^2$  fitting is not the only method used to obtain photometric redshifts. Lanzetta et al. (1996), for example, use the Maximum Likelihood estimator to find the best fitting SED, while Cabanac & Borra (1995) use a break-finding algorithm to identify discontinuities in the SED. All photometric redshift techniques rely on identifying strong features in the SED, and thus the  $\chi^2$  test will present a robust example. The advantages of the prism (higher spectral resolution and higher SNR in equal time) would achieve similar results with other redshift estimators.

### 3. Simulations

We performed Monte-Carlo simulations to test the use of prism spectra for photometric redshifts. Using the suite of input galaxy spectra with assumed redshifts and apparent K-band magnitudes, we generated 25,000 input galaxy SEDs. Then, using our photometric redshift software, we attempted to recover the input redshifts. In this section we describe each of these assumptions in detail.

Input spectra and comparison templates were chosen to differ slightly to simulate imperfect templates that will have to be used in realistic observations. The input spectra and the template spectra were taken from different ages for the same GISSSEL96 solar metallicity model. The exact spectra used are not meant to be a prediction of the SEDs of  $z > 5$  galaxies, but merely to be representative of the type of spectral breaks that might be encountered. The differences between the input and output are more important for this purpose than the difference of either model with (the currently unknown) reality.

To produce our simulated galaxy observations, we must assume a redshift distribution and an apparent magnitude distribution. We take our redshift distribution from the photometric redshifts of Fernandez-Soto et al. (1999) for the Hubble Deep Field North (HDF-N; see Williams et al. 1996). Since spectroscopy of HDF-N galaxies is currently limited to  $z < 6$ , we extend the distribution by extrapolating the existing number-redshift relation into the  $6 < z < 15$  range (see figure 2).

The flux distribution of the simulated galaxies is determined from the number-magnitude relation of the STIS observations of the HDF-South (Gardner et al. 2000). Those number counts are shifted to the K-band using a model of the median galaxy colors (Gardner 1998). The apparent magnitude distribution is sampled independently of the redshift distribution, but extremely unlikely luminosities are eliminated ( $L > 10L_*$  or  $L < 0.01L_*$ ).

The effect of Lyman forest blanketing is applied to the spectra as a final step. The  $\text{Ly}\alpha$  and  $\text{Ly}\beta$  decrements from Madau (1995) are applied, and flux is taken to be zero below  $912\text{\AA}$  in the rest frame, for galaxies at  $z > 2.5$ .

We then convolve the input spectra, with their redshifts and flux normalizations, with the response of either the filters or the prism. Prism response is modeled as a series of top-hat filters with widths corresponding to one resolution element. Depending on the



prism design (see section 3.2) the width of a resolution element in wavelength may vary as a function of wavelength. For comparison with camera-mode observations, we assume a logarithmically spaced set of filter wavelengths and widths, covering the  $0.6 - 5\mu\text{m}$  range. The filters were chosen to be Gaussian in shape. The filter widths were chosen so that each filter would overlap with its neighbor at the 30-40% throughput level and the filter next to that at the  $\sim 5\%$  throughput level. If the filters were much wider the measurement would be less distinct and spectral features (such as the  $4000\text{\AA}$  break) would be washed out. However, if the filters were much narrower there would be gaps between the filters and the dispersion of redshift errors would be large for galaxies with spectra breaks that fall in between the filters. Real filters (e.g. the WFPC2 filters – see Holtzman et al. 1995) are likely to be squarer but may have particular quirks (“red leaks”, etc.); we have chosen a simple filter profile as a baseline. Experiments with using “top-hat” filters have shown that it is the size of the gap between the filters (if any), not their exact shape, that dominates.

### 3.1. Instrument Properties and Noise Calculation

Photometric errors were calculated using a signal-to-noise estimator consistent with the Integrated Science Instrument Module (ISIM) Yardstick camera specifications (Greenhouse et al. 1999). Table 1 lists the parameters assumed. Specifications about the spectrometer are taken from the micro-shutter MOS study (Moseley et al. 2000). While imager specifications are taken from the Yardstick study, they are consistent with studies of other imagers (e.g. Bechtold et al. 2000).

Specifically, the imager is taken to be diffraction limited and critically sampled at  $2\mu\text{m}$ . This leads to a plate scale of  $0.036''/\text{pix}$ . Imaging observations are assumed to be background limited for the purposes of this study, although all noise sources (detector dark current and read noise, as well as Poisson noise in the objects) are include in the

model. The spectrometer, on the other hand, uses a coarser plate scale in order to preserve field of view. We assume the same physical detector characteristics (read noise and dark current), but a plate scale of  $0.1''/\text{pix}$  for the spectrometer. We assume that objects have size  $\sim 0.113''$  (i.e. a diameter that gives an encircled area of 8 square pixels in the imager for the full flux of the galaxy), broadly consistent with the estimates of Gardner & Satyapal (2000; see also section 4.3).

The signal to noise ratio for a simulated galaxy is determined by the following equations. For simplicity we assume that all detector pixels which contain any light from the object are treated equally.

$$S = s_\lambda \Delta\lambda A_{tel} \eta t \tag{1}$$

$$B_{zodi} = f_\lambda(\text{zodi}) \Delta\lambda A_{tel} \eta \Omega \tag{2}$$

$$\frac{S}{N} = \frac{S}{\sqrt{(B_{th} + B_{zodi})t + (I_{dark}t + R_N^2 \frac{t}{1000})N_{pix} + S}} \tag{3}$$

where:  $S$  is the signal in the object,  $s_\lambda$  is its flux density,  $A_{tel}$  the area of the telescope and  $t$  is the integration time. The  $\eta$  term is the instrument throughput, by which we mean the efficiency of the instrument only (optical elements and detector), with no angular dependence.  $B_{zodi}$  is the background from zodiacal light,  $\Omega$  is the solid angle of the admitted background (i.e. the area of the galaxy for imaging, or the area through the slit for the MOS), and  $N_{pix}$  the number of pixels in the object (for imaging) or the spectrum.  $B_{th}$  is the background from thermal emission by the telescope and the instrument (which is negligible at  $< 5\mu\text{m}$ ),  $I_{dark}$  is the dark current per pixel per second and  $R_N$  is the detector noise per readout. We assume the detector must be read every 1000 seconds due to the cosmic ray rate (Stockman 1997); if new data reduction techniques work around this (Offenberg et al. 1999), the read noise term will be smaller.

The throughput term,  $\eta$ , depends on the instrument design. Some absorption is suffered at each element in the optical path. For the imager, these elements are the mirrors

and the filters. Mirrors can easily be expected to have  $\eta \geq 0.95$  and filters should have  $\eta \geq 0.9$  at the peak. The MOS suffers an additional transmission penalty for the slit-array of  $\eta = 0.8$ . There is an additional loss for the detector quantum efficiency ( $QE \sim 0.8$ ); we neglect a small wavelength dependency in this term. In this study we used  $\eta = 0.41$  for the imager and  $\eta = 0.35$  for the MOS.

For filter imaging, in background limited imaging, the sensitivity of serial observations scales inversely with the bandwidth of the filters. That is, for fixed total observing time for all filters, signal-to-noise is decreased by the square root of the time per filter *and* by the square root of the decrease in signal from the narrower filter bandwidth, so that  $S/N \propto 1/N_{\text{filters}}$ .

### 3.2. Prism Resolution

The prism-mode sensitivity is a function of the varying resolution across the wavelength range, in addition to the zodiacal light and detector noise characteristics. The properties of available materials do not provide a constant resolution across  $0.6 - 5\mu\text{m}$ , with a preliminary design resolution vs. wavelength curve shown in figure 3. We expect further study of prism properties may produce a more optimal prism, with a somewhat flatter dispersion curve..

### 3.3. Figures of Merit

Once we perform the recovery of simulated redshifts, we must have criteria by which to judge our success rate. Two considerations influence the choice of the figure of merit: the usefulness of the recovered redshifts, and the sensitivity of the figure of merit to changes in the simulations.

The first point is that at larger redshift, a larger deviation in redshift is likely to be acceptable. SED-fitting will not recover redshifts with the precision of higher resolution ( $R \sim 1000$ ) spectroscopy, so the study of small scale galaxy clustering and physical interactions will not be possible. An absolute redshift error,

$$\delta_z = |z_{phot} - z_{true}| = \text{const}, \quad (4)$$

is not the right definition of success. Instead, we need something that grows with redshift. Redshift recovery errors are sometimes expressed in terms of percent of redshift,  $\delta_z/z$ . In the case of our simulations, that criterion grows too fast with redshift and almost all results would be classified as successes. Also, while a result of 3% may be sufficient to tell that a galaxy is at high redshift, it may not be sufficient to do certain kinds of science (see for example section 5.2). Instead, we examined the results of the simulations (see figure 4) and chose the slowly growing function

$$\delta_z < 0.03 + 0.1 \times \log z \quad (5)$$

to be the boundary at which we define success (with a minimum  $\delta_z = 0.03$ ; that is, we do not use the  $\log$  term when  $\log(z)$  is negative).

We define a large error in redshift recovery as a catastrophic failure. Such failures occur when one strong break in the SED is aliased to another (for example confusing the Lyman break with the  $4000\text{\AA}$  Balmer break). Following the same logic used for successes, we define a catastrophic failure to be an object for which

$$\delta_z > 0.50 + 1.0 \times \log z \quad (6)$$

with a minimum of 0.5.

For each run of the Monte Carlo simulations we will count the number of successes and catastrophic failures. Metaphorically, successes are darts which hit the bullseye and catastrophic failures are darts that miss the board entirely.

At this stage of the study, we compare prism and filter observations of the same objects, without regard to MOS selection; in section 5.1, we will consider the penalty the prism pays for needing an input mask.

## 4. Results

Figures 5 and 6 shows the output of the simulations for the nominal prism compared to 10 filters in the Yardstick imager. We clearly see that the imager suffers by dividing the total exposure time between the filters. The distribution of  $\delta_z$  is wider for the imager, leading to fewer successes and a wider error distribution at high redshifts. In particular, the prism measures 68% of the galaxies with excellent accuracy (successes according to section 3.3), while the filters only measure 42%. The disparity is even greater at high redshifts ( $z > 4$ ), where the prism has an 89% success rate, while filters succeed on only 46% of the objects. If we consider only the faintest ( $K > 30$ ) objects at high redshift, the difference is 80% to 33%.

In the following sections we vary some of the underlying assumptions of the simulations to test the robustness of this result.

### 4.1. Optimal Resolutions

When obtaining redshifts from SED fitting, there is an advantage to having higher resolving power. To detect a break in the continuum one needs to have 3 resolution elements – one below the break wavelength, one encompassing it, and one above it. Hence to be sensitive to breaks at a wide range of redshifts, numerous resolution elements are needed. Further, the narrower the resolution element, the more precisely the wavelength of the break can be inferred. However, in serial observations there is a trade off between resolving

power and exposure time per filter, in the case of fixed total exposure time. With a prism, there is no such trade off for a single object (as long as the observations are background limited), but there is a point of diminishing returns.

We first investigated the question: what is the optimal resolution for medium-band filters to obtain photometric redshifts. We ran Monte Carlo simulations for a series of filter resolutions with a fixed total exposure time of  $10^5$  seconds. Averaged over all redshifts and all magnitudes, 30 filters produce somewhat better photometric redshift estimates. However, the advantage of 30 filters over 10 is not large. It is more likely that in a real imager, ten medium/wide band filters would be the limit of available space in the mechanism (some slots in filter wheels being reserved for narrow-band filters, etc.).

Prism resolving power may also affect the success rate in recovering redshifts. We ran our simulations for various prism resolutions assuming that the shape of the  $R$  vs.  $\lambda$  curve did not change, only the minimum  $R$ . Figure 7 shows the success and failure rates for prisms of varying resolving power. We note that the nominal prism resolving power ( $R \sim 55$  at  $1 \mu\text{m}$ ) is, in fact, the point of diminishing returns. The reason for this plateau is that detector noise becomes important at  $R \gtrsim 100$  for the instrument parameters that we have assumed.

We also investigated a prism that has the same resolving power at all wavelengths, even though such a “flat prism” is not technically achievable. We found that there was no significant advantage to a flat resolution curve. In a similar tactic, we also experimented with binning the resolution elements at the short wavelength end (in “post processing”, not “on chip”) to get a “flatter” prism; as expected, this had little effect, since binned data in the  $\chi^2$  fitting are statistically equivalent. The only case in which binning would matter greatly would be in a detector noise limited case, and then the binned data would be worse than unbinned data at lower resolution (since higher resolution means the spectrum extends

over more detector pixels).

#### 4.2. Effect of Different Input and Output Templates

Accurate measurement of redshifts from SED-fitting relies on having a very good comparison template set. However, in modeling the results, we must take into account that no template set could be perfect. We therefore need to check that our templates are different enough from our input galaxy spectra.

We ran the simulations using *exactly* the same input and output spectra (see figure 8). Artificially good results are obtained. The  $\chi^2$  fitting is very sensitive to recovery of the same spectrum. This advantage is seen in the anomalously accurate results for the lowest number of filters. When using the same input and output spectra, it appears that lower resolution is better. To match an exact template set, less resolution is required and so the signal to noise advantage of  $N_{\text{filters}} = 10$  dominates. However, it is unlikely that, even with principal component analysis, an exact template set can be constructed for an arbitrary deep field. We proceed with confidence that our input templates are sufficiently different for purposes of the simulation, as they still show an advantage to greater resolution.

Also, we note that since we are not trying to model the actual spectra we might see, we have not included the effect of extinction. However, extinction produces a change in the slope of the SED, as does age. We are confident that our ability to match up SEDs of different ages indicates that the same procedure would be effective when applied to different extinctions. Extinction is well handled in most modern photometric redshift algorithms, so there is no reason to expect that it would be a problem here.

### 4.3. Plate Scale and Slit Width

A critical difference between the imager and MOS designs that are currently being considered is the plate scale at the detector. The imager design is driven by a balance between spatial resolution and field of view. The MOS has at least two different modes: a moderate resolution diffraction grating mode for the key spectroscopic observations ( $R \sim 1000$ ), and a low resolution ( $R < 100$ ) prism mode for photometric redshifts. The choice of MOS plate scale will be driven by the signal to noise considerations in the primary  $R \sim 1000$  mode. In that regime, detector dark and read noise will be dominant over the zodiacal background, and it is desirable to collect the light from a galaxy into as few detector pixels as possible while maintaining adequate sampling. In addition, the MOS may need to devote detector pixels to area outside the field of view (to avoid edge effects in the dispersed spectra). As a result, the SNR would suffer and field of view would be lost in the grating mode if the same plate scale were maintained as the imager, so a coarser plate scale is preferred. The micro-shutter MOS has a slit width of  $0.2''$  sampled by detector pixels of  $0.1''$ . The background limited prism will pay a penalty for the choice (for sources of angular size smaller than the 2 pixel sampling size), since pixels that subtend larger solid angle will detect more zodiacal light. Of course, for extended sources the finer plate scale has less advantage.

The effect that the plate scale has on the SNR depends on the sizes of the faintest galaxies. Current galaxy observations of the HDF-N and HDF-S reach magnitudes of  $AB = 30$ . With NGST, we expect to reach ten times fainter with prism spectroscopy. The deepest image ever taken is the STIS CCD image of the HDF-S, which sees some galaxies at  $AB > 30$  (Gardner et al. 2000). These faintest galaxies are barely resolved at the STIS resolution, with half-light radii of 0.1 arcsec. After correcting for the effects of the point spread function on the STIS and NICMOS images, Gardner & Satyapal (2000) show



that galaxy sizes in the NIR are smaller than in the visible, perhaps because the bulges of galaxies become more prominent at longer wavelengths. We have assumed a diameter  $\sim 0.113''$  (see Section 3.1), in order not to overestimate the zodiacal background penalty suffered by filter imaging.

Figure 9 shows the effect of assuming different galaxy sizes on the recovery of redshifts with 10 filters. The galaxy size matters, as expected. However, the effect is not large, and galaxies have a distribution of sizes, so our assumption seems acceptable.

#### 4.4. Detector Noise

Detector noise is an important factor in the signal to noise calculation. With our assumptions about the likely state of detector technology,  $R \sim 100$  prism spectroscopy would be detector noise limited. As a result, there are diminishing returns for increasing prism resolution, since more resolution elements mean more detector pixels and hence more noise. On the other hand, detector technology could improve more than we are assuming. If the detector noise (the combination of dark current and readout noise) were to improve by a factor of  $\sim 5$ , then  $R = 100$  spectra would be background limited at all wavelengths. That is, the zodiacal background noise would exceed the detector noise at all wavelengths. With the current detector parameters, the detector noise is equal to about the average of the zodiacal background (which is highly variable with wavelength, with a local maximum at  $2 \mu\text{m}$ , a local minimum at  $\sim 3.7 \mu\text{m}$ , and a rise towards longer wavelengths).

A higher resolution prism could be advantageous. At  $R \sim 100$  it would be possible to detect strong emission lines. Ground based instruments like NIRC on Keck I (see Matthews & Soifer 1994) currently obtain emission-line spectra of  $z > 2$  galaxies with  $R = 100$  grism spectroscopy.

If emission-line spectra were possible, redshift measurement would be vastly improved. In the difficult  $1 < z < 3$  regime, strong optical emission lines shift into the NIR passbands.  $H\alpha$ ,  $H\beta$ , [OIII], and [OII] could all be accessible. Low resolution NIR spectroscopy has successfully identified galaxies on the basis of  $H\alpha$  with NICMOS onboard HST (see McCarthy et al. 1999). At higher redshifts,  $Ly\alpha$  might be observable, significantly strengthening the believability of the redshifts obtained with the prism.

$R \sim 100$  spectra would not be able to measure line-widths, but the wavelength and strength of the lines would be accessible. These would be particularly useful for the many objects which might not be observable by other instruments. Recall, though, that high signal to noise,  $R \sim 100$  prism spectroscopy may require better detectors than are currently predicted using the most conservative assumptions.

## 5. Discussion

For a single object, the advantage of a prism over medium-band filters is clear – it measures the entire wavelength range simultaneously. Integration time per filter goes down as spectral resolution increases for serial filter observations. Thus, at first glance, one might expect an advantage for the prism equal to the square root of the resolution. An ideal  $R = 25$  prism might recover redshifts  $\sqrt{25} = 5$  times more efficiently than filters. In reality, the restrictions imposed on the MOS design by the primary grating mode would decrease this advantage. Figure 10 shows the advantage of prism observations over filter observations as a function of magnitude. We see that the advantage of the prism is greatest for the fainter objects. The prism achieves an excellent fit for twice as large a percentage of objects than the best filter case (10 filters).

To put this another way, prism observations will reach fainter galaxies in the same

observing time and resolution for a fixed  $\delta_z$ . They will also recover a more complete sample of redshifts (depending on the constraints of the MOS selection). This extra depth is the critical point to understanding why a prism is the right mode for photometric redshifts. The primary discovery space of NGST will be at the faintest magnitudes and the highest redshifts.

Catastrophic failures are an important consideration in judging the effectiveness of a photometric redshift technique. Since observers of a deep field do not know *a priori* the redshifts of the observed galaxies, they rely on the SED fitting. Clearly, then, it is important to know at least that the redshift estimates have the correct trend, if not exactly the right answer. It is important to avoid labeling  $z < 3$  galaxies as the first light from  $z > 10$  proto-galaxies (see for example figure 4). In figure 11 we examine the number of “interlopers” suffered in recovered redshifts. We define any galaxy that is misidentified by  $\delta_z > 1$  as an interloper, a slightly different definition than our “missing the dart board” criteria from section 3.3. The ten filters case has  $\sim 30\%$  interlopers at  $z > 10$ , causing considerable confusion. The cause of the interlopers is likely to be the misidentification of a feature as the Lyman break when it is actually a longer wavelength spectral break at a much lower redshift. This effect is especially pernicious at the faintest magnitudes.

On the other hand, the Lyman break is the most easily identified feature. For all but the catastrophic failures, the distribution of  $\delta_z$  is more sharply peaked at higher redshifts. In figure 12 we show the recovery rates for faint objects at  $z > 4$  as a function of magnitude. The prism advantage is clearly largest in this regime, especially at the faintest flux levels. We must keep in mind that these objects will *only* be observed with low resolution modes – an  $R \sim 1000$  spectrograph is unlikely to reach such faint depths for continuum spectra. It is therefore important to obtain the maximum possible information from the SED, by minimizing  $\delta_z$ .

### 5.1. Completeness in MOS Observations

The prism’s ability to accomplish the core science goals also depends on the number of targets that can be measured in each mode, as well as the accuracy of the recovered redshifts. Since prism spectra will take up only a fraction of the pixels available in each row, the low resolution mode will be able to accommodate many spectra in each row and achieve a high degree of completeness at the magnitudes of interest (see Moseley et al. 2000). An additional optimization is possible with prior selection based on photometry in a single band (which would be necessary for aperture assignment, in any event). We also note that many, if not most, science applications will not require spectra of every object.

For example, in the Moseley et al. (2000) micro-shutter MOS,  $\sim 6000$  apertures are available for prism spectra over a  $3.75 \times 7.5$  arcminute field of view. Down to  $K_{AB} < 32$ , there are 33,200 galaxies (using the number counts model of Gardner 1998). Of these galaxies, 15,400 have  $K_{AB} > 30$ . Several galaxies can fall close together within the same row meaning that only one can be selected at a time by the MOS. Thus, in multiple exposures with different MOS selections, there may be a diminishing number of uniquely selectable galaxies each time. For randomly distributed galaxies at  $K_{AB} > 30$ , 5500 of the 6000 MOS apertures will have at least one galaxy available, while 4400 will have at least two, 2800 have at least three and so on. Thus, in two  $10^5$  second exposures, the MOS could obtain spectra of 64% of the  $30 < K_{AB} < 32$  galaxies in the field of view, and 93% could be observed in 4 exposures (see Gardner & Satyapal 2000 for more discussion of the efficiency of MOS slit use). Since we assume that long exposures will be made by the coaddition of numerous  $\sim 1000s$  exposures, the MOS could be re-configured several times within each pointing, allowing an optimization of the total exposure time for each galaxy. Thus, the brighter galaxies could be observed with shorter exposures within the same 4 long integrations, reducing the confusion problem. We expect that future studies will use

artificial intelligence techniques to assign slits to galaxies, making the most efficient use of the exposure time.

Number of objects measured, however, is not the only factor in evaluating the prism vs. the filters; the crucial additional factor is the accuracy of the measurements. It is important not to have a large number of “interlopers” in the measured sample (see figure 11 and the discussion above). While the filters measure twice as many “proto-galaxies”, up to 40% of them may be false identifications. Similarly, for galaxies that are not interlopers, it is important to measure them as accurately as possible. Again, we note that for the faintest galaxies there will be no additional spectroscopic followup. Faint, high redshift galaxies are the prime discovery space for NGST.

Since the MOS may not be able to select all the objects of interest in a single spectroscopic observation, the prism vs. filter comparison should, perhaps, give more observing time to the filters (which can get all the objects at once). Figure 13 shows that even with substantially more integration time, 10 filters are not able to achieve the narrow error distribution possible with the prism.

## 5.2. Science Example

How important is the prism’s advantage in achieving a narrow error distribution in redshift measurement? Certainly the 10 filter case does measure many high redshift galaxies with fair accuracy. The importance of more accurate redshifts lies in the fact that at the faintest magnitudes most redshifts will not be confirmed by higher resolution spectroscopy from NGST or the ground. One example of science with redshifts good to a few percent is to look at the gross features of large scale structure. Prism redshifts will show the statistical presence of large scale structures in the redshift distribution, while redshifts measured with

10 filters may not.

The local (low redshift) universe shows a great degree of large scale structure in galaxy redshift surveys (e.g. Huchra, Vogeley & Geller 1999), having “Great Walls” (e.g. Geller & Huchra 1989) and “Voids” (e.g. Kirshner et al. 1987). One would like to test to see if similar structures exist in the early (high redshift) universe. Such a measurement would require large numbers of accurately measured redshifts at high redshift. Without higher resolution spectroscopic followup, can we see a void in the galaxy redshift distribution?

To test this question, we have created an artificial “flat” galaxy distribution with a high contrast void at  $z = 6$ . The void is 5000 km/sec in width (Kirshner et al. 1987, Jones & Fry 1998) and completely empty with large numbers of galaxies in front of and behind it. Lower contrast voids would be harder to detect, so this is a “best-case” scenario. However, the intent in this experiment is not to model a realistic void (which might have at most a factor of two underdensity), but merely to see what effect the accuracy of redshifts measured with a prism/MOS vs. serial filters would have on our ability to detect such structures.

Each galaxy redshift was changed by an amount,  $\delta z$ , randomly sampled from the distribution of  $z_{true} - z_{phot}$  shown in figure 13. The distribution was sampled for the nominal prism and for the 10 filter case with twice the exposure time (to allow the MOS two “shots” to measure sufficient galaxies). The results are shown in figure 14. There is a slight dip at  $z \sim 6$  for the filter case, but it is indistinguishable from the regular  $1\sigma$  fluctuations in the distribution. It would be difficult if not impossible to know that even such a high contrast void had been detected if these were the only redshift measurements available. On the other hand, the significant underdensity in the prism/MOS case is unmistakable.

The added accuracy provided by higher resolution SEDs that is possible with a prism, without sacrificing signal-to-noise, may be critical in our ability to detect large scale

structure in the galaxy distribution at high redshift.

## 6. Conclusions

We have run Monte-Carlo simulations to assess the utility of using a low resolution prism with a MOS on NGST to measure large numbers of galaxy redshifts. Each simulation consisted of 25,000 galaxies ranging in redshift from  $0 < z < 15$  and having  $26 < K_{AB} < 32$ . Simulations were run for a prism in the micro-shutter MOS and filters in the Yardstick Imager (similar results would be obtained for the micro-mirror MOS as well). We varied the prism resolution (and shape); the number of filters; the size of the galaxies and the total exposure time (for the filters); and how well the SED templates matched the input simulated SEDs. We reached the following conclusions:

- In all cases the prism/MOS gives a superior result. The percentage of excellent “measured” redshifts is a factor of 2-3 times higher than that obtained with the filters. The percentage of interlopers which would contaminate high redshift samples is about a factor of 2 lower with the prism.
- In the regime where much of the core NGST science will be done (very faint, very high redshift galaxies), the prism gives much more accurate and reliable redshifts. The filters, by contrast, suffer a large number of interlopers ( $\delta_z > 1$ ), up to 40% around  $z = 10$ . In this most important regime, higher resolution spectroscopic follow-up would be difficult or impossible.
- The accuracy and reliability of the prism in determining redshifts does not vary much with prism resolution in the background-limited regime. If detector noise could be reduced more than currently planned, higher resolution prism spectroscopy ( $R \sim 100$ )

could measure redshifts with both SED-fitting and through detection of strong emission lines.

- Redshift recovery is highly dependent on good signal-to-noise measurements of the SED itself. Thus the results for large numbers of filters are very poor. The increased resolution does not make up for the decrease in the signal to noise ratio caused by the division of total exposure time among many filters. Therefore, the imager cannot achieve the resolution and accuracy of the prism in a reasonable integration time.

We acknowledge useful discussions with Matt Greenhouse and John Mather. Sophia Khan worked on an earlier version of the simulations. HIT received support for this work from the STIS IDT through the National Optical Astronomical Observatories and by the Goddard Space Flight Center.



## REFERENCES

- Bechtold et al. 2000, to appear in “NGST Science and Technology Exposition”, eds. E.P.Smith & K.S. Long
- Brunner, R. J., Connolly, A. J., Szalay, A. S. & Bershad, M. A., 1997, *ApJL*, 482, L21
- Bruzual, A. G. & Charlot, S., 1993, *ApJ* 405, 538
- Buckham, B., Erickson, D., Nahon, M., Sharf, I., & Crampton, D., 2000, to appear in “NGST Science and Technology Exposition”, eds. E.P.Smith & K.S. Long
- Cabanac, R. & Borra, E.F. 1995, *PASP*, 108, 271
- Coleman, G. D., Wu, C. C., & Weedman, D. W., 1980, *ApJS*, 43, 393
- Connolly, A. J., Szalay, A. S., Dickinson, M., Subbarao, M. U., & Brunner, R. J., 1997, *ApJL* 486, L11
- Fernandez-Soto, A., Lanzetta, K. M., & Yahil, A., 1999, *ApJ* 513, 34
- Gardner, J.P, 1998, *PASP*, 110, 291
- Gardner, J.P, et al., 2000, *AJ*, 119, 486
- Gardner, J.P. & Satyapal S., 2000, *AJ* submitted
- Geller, M.J. & Huchra, J.P. 1989, *Sci* 246, 897
- Giallongo, E., D’Odorico, S., Fontana, A., Cristiani, S., Egami, E., Hu, E., & McMahon, R. G., 1998, *AJ*, 115, 2169
- Good, J., et al. 1994, in “IRAS sky survey: Explanatory Supplement”, JPL
- Graham, J.R., Abrams, M., Bennett, C., Carr, J., Cook, K., Dey, A., Najita, J., & Wishnow, E. 1998, *PASP*, 110, 1205
- Greenhouse, M. A., 1999, *BAAS* 194.9113
- Hogg, D.W. et al., 1998, *AJ* 115, 1418

- Holtzman, J. A., et al. 1995, PASP, 107, 156
- Huchra, J.P., Vogeley, M.S. & Geller, M.J., 1999, ApJS 121, 287
- Jones, M.A. & Fry, J.N., 1998, ApJL 500, L75
- Kirshner, R.P., Oemler, A. Jr., Schechter, P.L., & Shectman, S.A., 1987, ApJ 314, 493
- Koo, D.C., 1985, AJ 90, 418
- Lanzetta, K. M., Yahil, A., & Fernandez-Soto, A., 1996, Nature, 381, 759
- Le Fevre, O., et al. 2000, to appear in “NGST Science and Technology Exposition”, eds.  
E.P. Smith & K.S. Long
- MacKenty, J.W. et al. 2000, to appear in “NGST Science and Technology Exposition”, eds.  
E.P. Smith & K.S. Long
- Madau, P., 1995, ApJ 441, 18
- Mather, J., et al. 2000, SPIE, in press
- Matthews, K., & Soifer, B. T. 1994, in *Infrared Astronomy with Arrays: The Next Generation*, ed I. McLean (Dordrecht: Kluwer), 239
- McCarthy, P.J., et al. 1999, ApJ, 520, 548
- Moseley, S.H. et al. 2000, to appear in “NGST Science and Technology Exposition”, eds.  
E.P. Smith & K.S. Long
- Offenberg, J.D., Sengupta, R., Fixen, D.J., Stockman, P., Nieto-Santiseban, M., Stallcup, S., Hanisch, R., & Mather, J.C., 1999, *Astronomical Data Analysis Software and Systems VIII*, ASP Conference Series, Vol. 172. Ed. D. M. Mehringer, R. L. Plante, & D. A. Roberts. ISBN: 1-886733-94-5 (1999), p. 141.
- Oliva, E., 1999, XLIII SAIT national conference proceedings, Mem. Soc. Astr., in press
- Roberts, S. et al., 2000, to appear in “NGST Science and Technology Exposition”, eds.  
E.P. Smith & K.S. Long

Stiavelli, M. 1998, private communication

Stockman, H.S., 1997, ed., “Next Generation Space Telescope: Visiting a Time When Galaxies Were Young”, (AURA, Inc.: Baltimore)

Wheelock, S.L., et al. 1994, in “IRAS sky survey: Explanatory Supplement”, JPL

Williams, R.E. et al., 1996, AJ, 112, 1335

Williams, R.E. et al., 2000, AJ, in preparation

Table 1. Detector and Noise Characteristics

Zodiacal light estimate	Stiavelli 1998 <sup>a</sup>
Dark Current	$0.02e^-/\text{sec}/\text{pixel}$
Read Noise	$4e^-$ rms
QE	80%
Diffraction Limit	$2\mu\text{m}$
Imager Plate Scale	$0.0036''/\text{pix}$
Spect. Plate Scale	$0.1''/\text{pix}$

<sup>a</sup>The zodiacal light calculation of Stiavelli 1998 is based on the model of background light fit to IRAS data by Good et al. (1994) and Weelock et al. (1994). We assume the observation is made at the ecliptic pole.

Fig. 1.— The GISSEL96 galaxy templates used in the simulations. We used a 1 Gyr burst, with solar metallicity. The 10 spectra cover the age range from 0.8 to 11 Gyr. For most of the simulations, 10 similar yet distinct spectra at intermediate ages were used to make the model redshifted galaxies, so that the simulated input data differed slightly from the templates.

Fig. 2.— The redshift distribution of simulated galaxies, derived from the distribution of photometric redshifts of faint galaxies in the HDF-N compiled by Fernandez-Soto et al. 1999

Fig. 3.— The resolution as a function of wavelength for the near-IR prism. The minimum resolution can be selected to meet science goals; this figure shows the resolution of the nominal prism, but the minimum value (where  $R=25$  on this figure) could be changed, without changing the relative shape of the plot.

Fig. 4.— The results of one simulation. In this simulation, 10 filters were used to sample the model spectra and the templates in a  $10^5$  second observation. The solid lines represent the criteria for an excellent fit, “hitting the bulls-eye”. The dashed lines represent the criteria for an unacceptable fit, “missing the dart board”.

Fig. 5.— The results of the simulations as recovered redshift vs. input redshift are shown for top: the nominal (10) filter case, and bottom: the nominal prism. In both cases a  $10^5$  second observation was assumed. The successes and failure lines are shown as solid and dashed lines, respectively. Notice that some galaxies with redshifts between  $z=1$  and  $z=3$  are problematic for redshift recovery and that the percentage of catastrophic failures is much higher for the filters. Also, the relation between measured redshift and true redshifts is good for both the prism and the filters at  $z > 4$ , but the prism has a narrower distribution.

Fig. 6.— A histogram of the error distribution ( $z_{true} - z_{phot}$ ) for objects at  $z > 4$ , for the

results of the simulation shown in figure 5. Not shown are the “interlopers”; that is, objects with  $|\Delta z| > 1$ .

Fig. 7.— The effect of varying prism resolution is shown for all simulated galaxies (open circles), and those galaxies at the faintest 2 magnitudes (filled circles), in  $10^5$  second observations..

Fig. 8.— The effect of simulating galaxies with input spectra exactly the same as the comparison templates is shown (open circles) in comparison with the results using our adopted input spectra (filled circles).

Fig. 9.— The dependence of redshift recovery on galaxy size is shown. The data points show the results of the simulation in the 10 filter case for successively larger apertures, in  $10^5$  second observations.

Fig. 10.— The success rate for the nominal prism (dot-dash line), the 10 filter case (dotted line) and the 40 filter case (thin line) compared to the total simulated galaxies (thick line). Successes are defined as in section 3.3.  $10^5$  second observations are assumed in each case. Notice that the higher resolution and signal to noise of the prism are of great advantage at faint magnitudes, but the resolution of 40 filters is overcome by the signal to noise advantage of ten filters at  $K = 29$ . Also, note that these results assume galaxies have a diameter  $\sim 0.113''$ ; if galaxies were larger the prism would have a greater advantage.

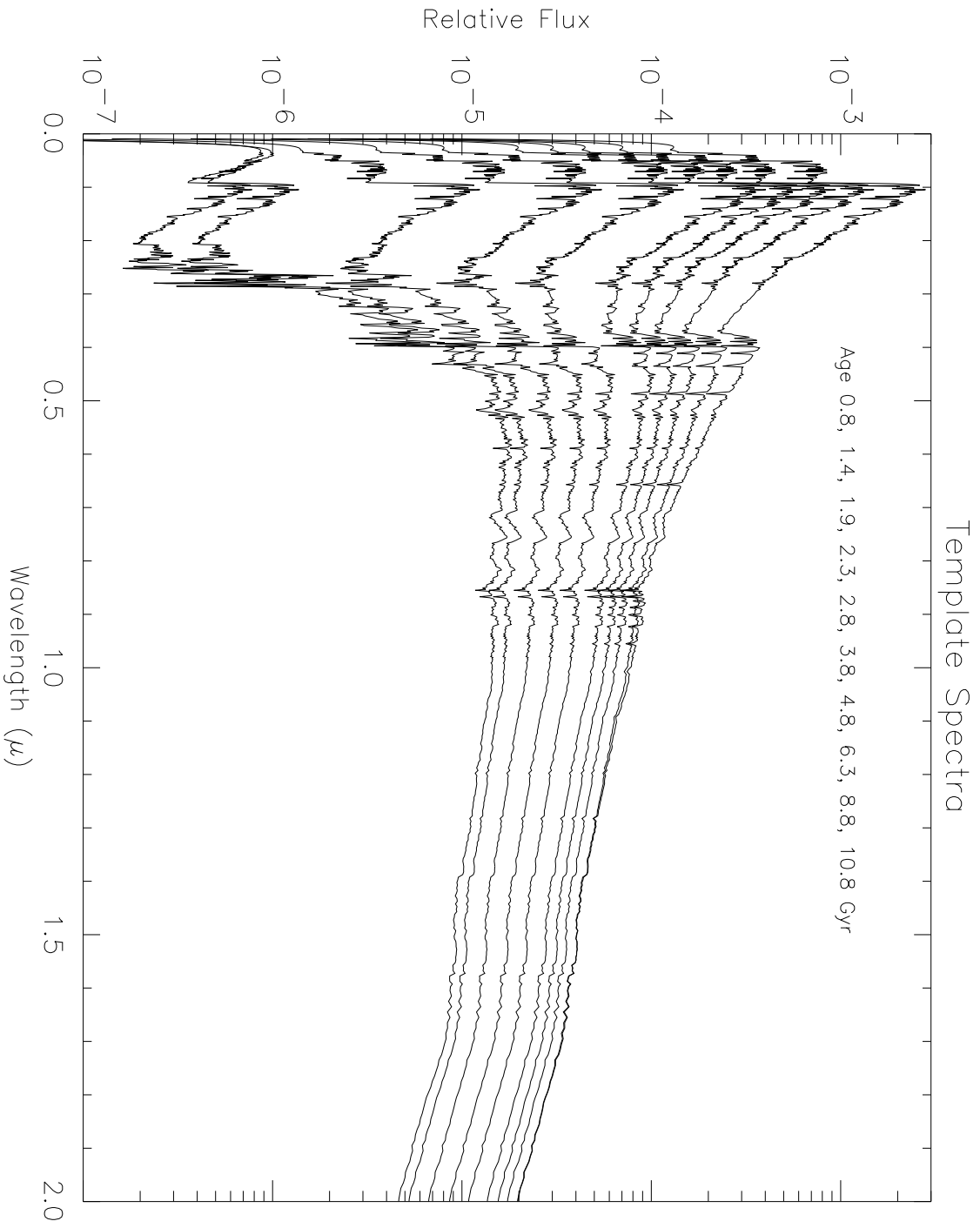
Fig. 11.— The percent of measured redshifts which will fall into the wrong unit  $z$  bin (interlopers) is shown for the prism (dashed line) and for the 10 filters case (solid line), in  $10^5$  second observations. Most of the interlopers with photometric redshifts of  $z > 5$  come from galaxies at  $1 < z < 3$ .

Fig. 12.— As in figure 10, but limited to galaxies with input redshifts greater than  $z=4$  (the

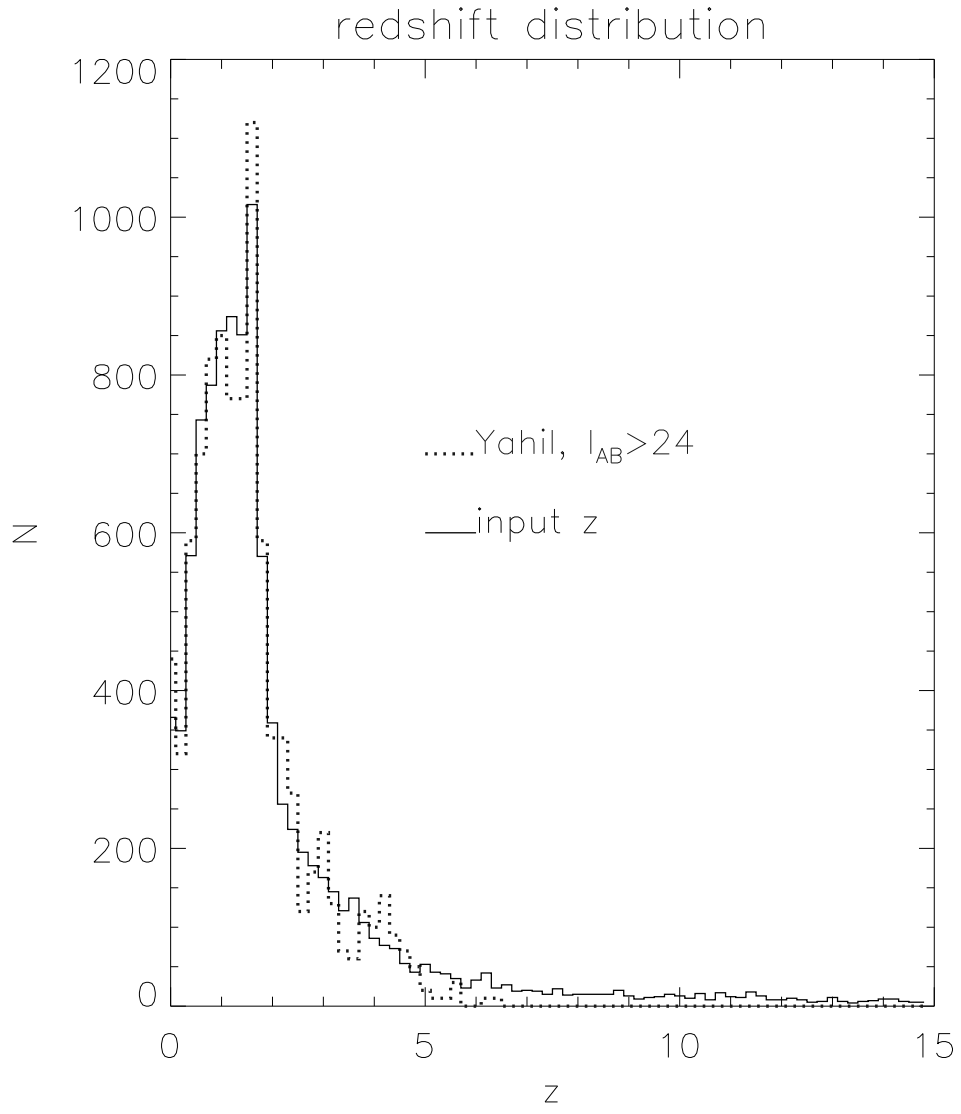
key discovery space for NGST).

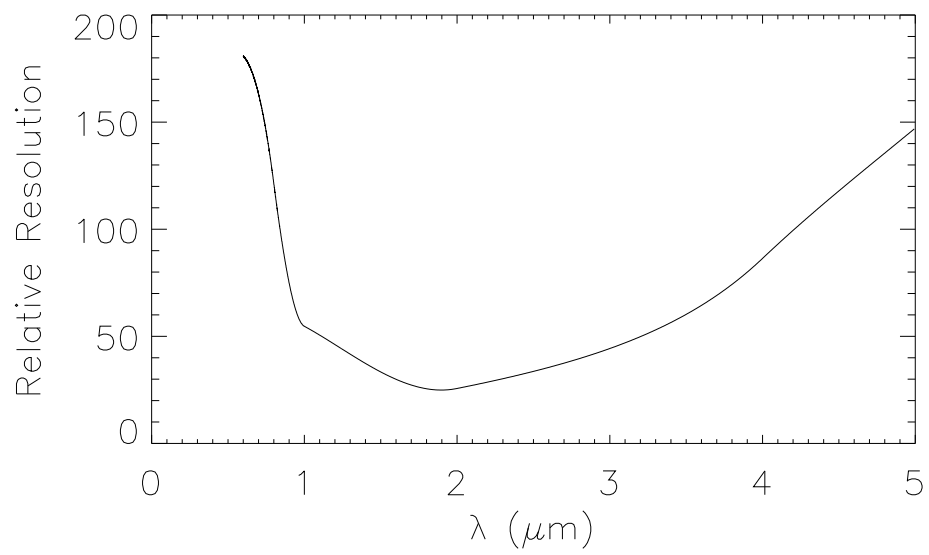
Fig. 13.— The effects of increasing the total exposure time for the filters is shown. For each total exposure time we plot the width of the error distribution for high redshift ( $z > 4$ ) objects. Not shown are the “interlopers” (see figure 11).

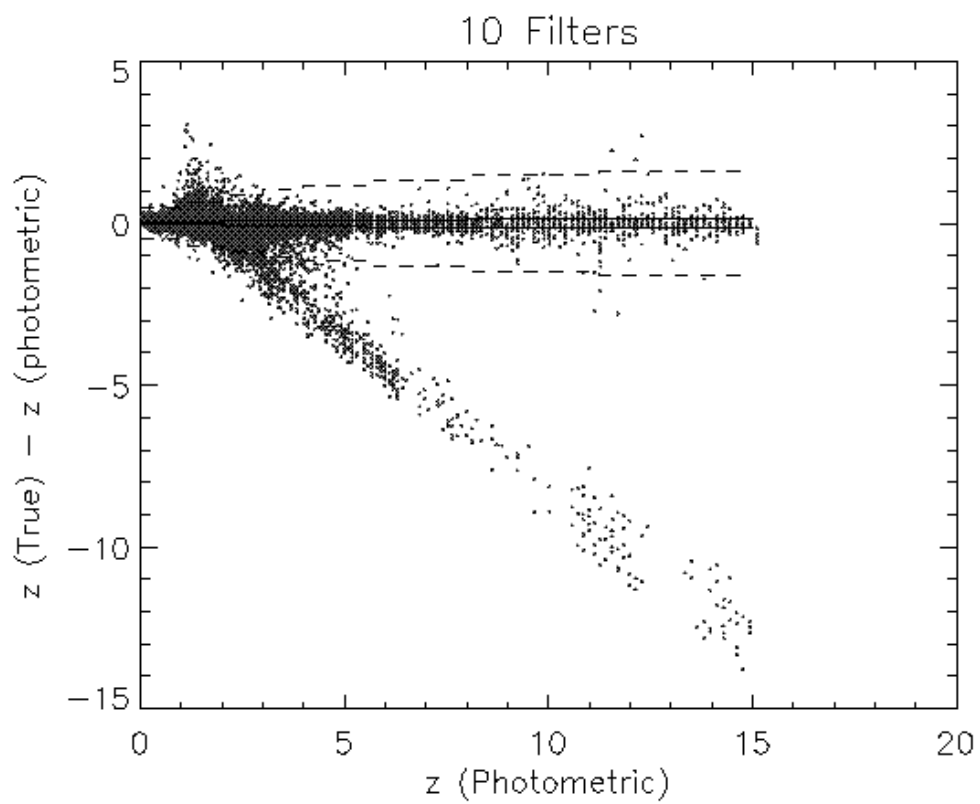
Fig. 14.— A redshift distribution containing a  $z = 6$  void with 5000 km/sec width. The bottom histogram (displaced downward for clarity) is the input redshift distribution. The middle histogram (also displaced) is the distribution sampled with the accuracy of the prism/MOS, and the top histogram is the distribution sampled with the accuracy of 10 filters.

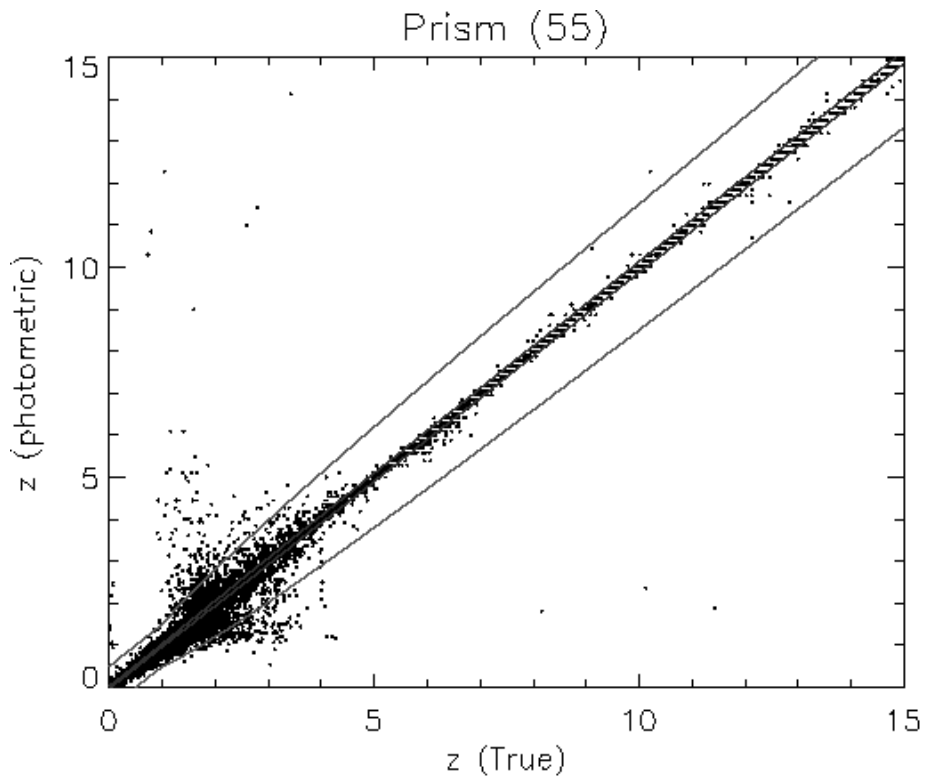
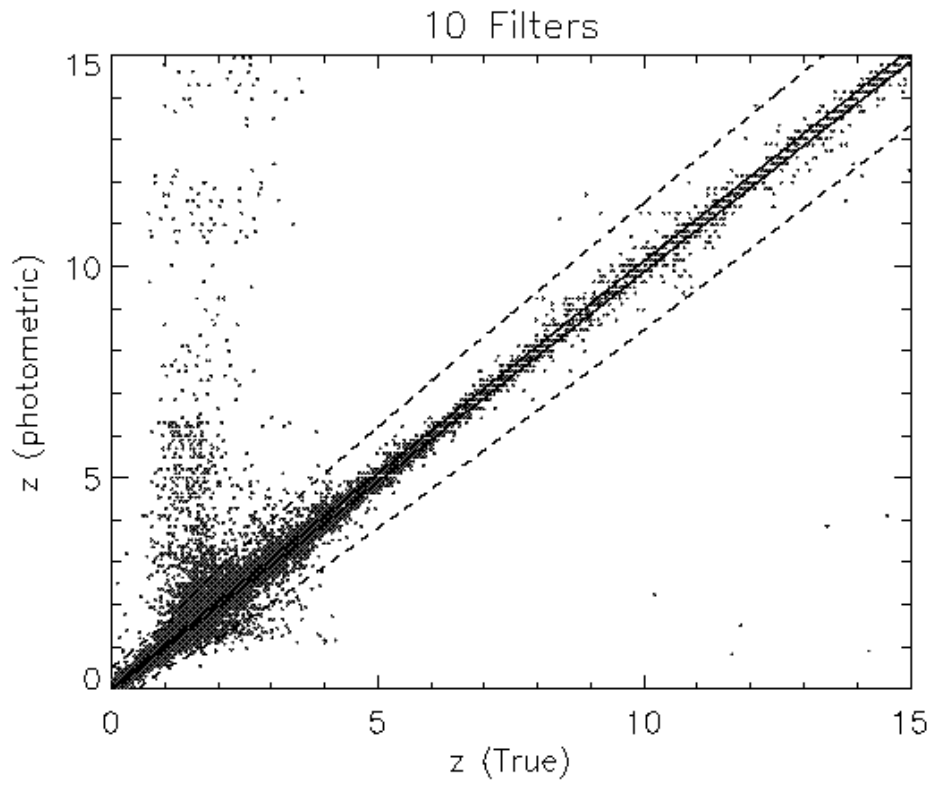


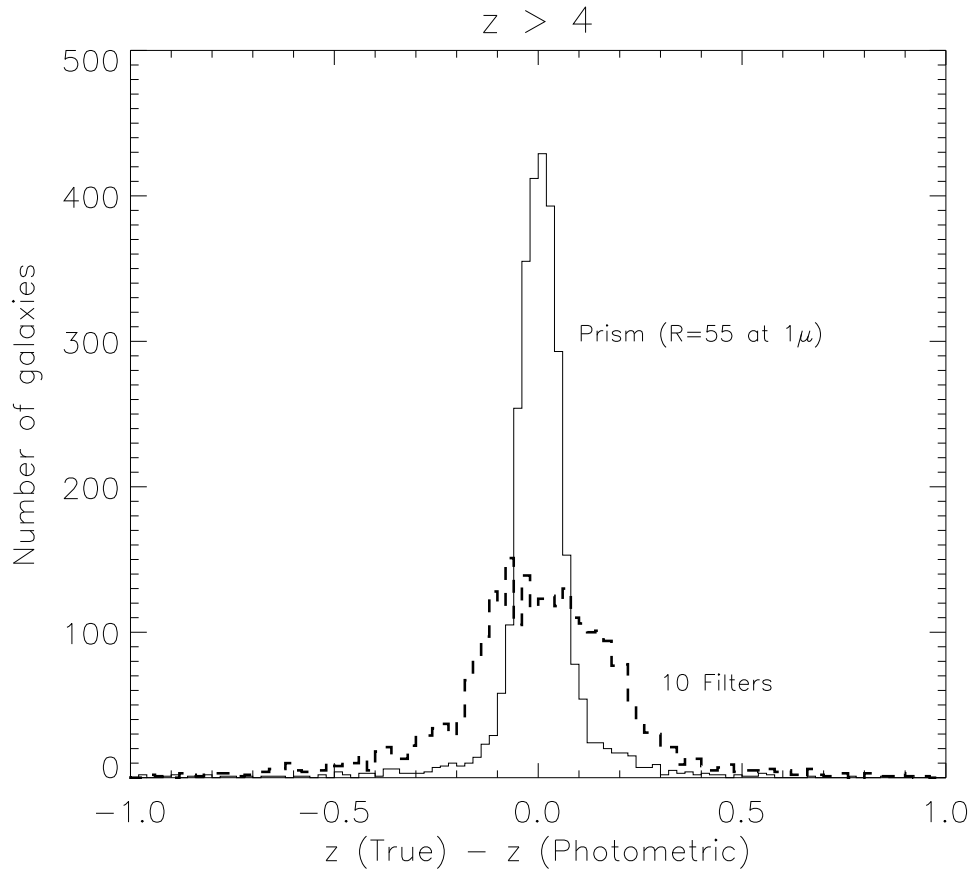


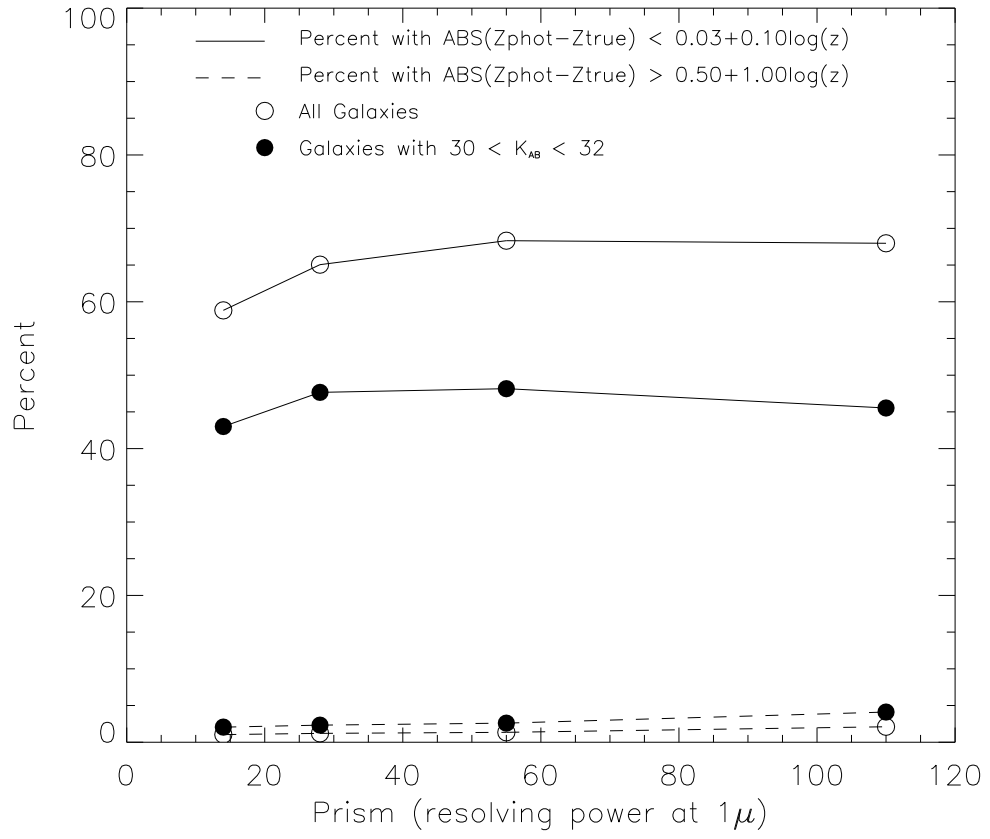


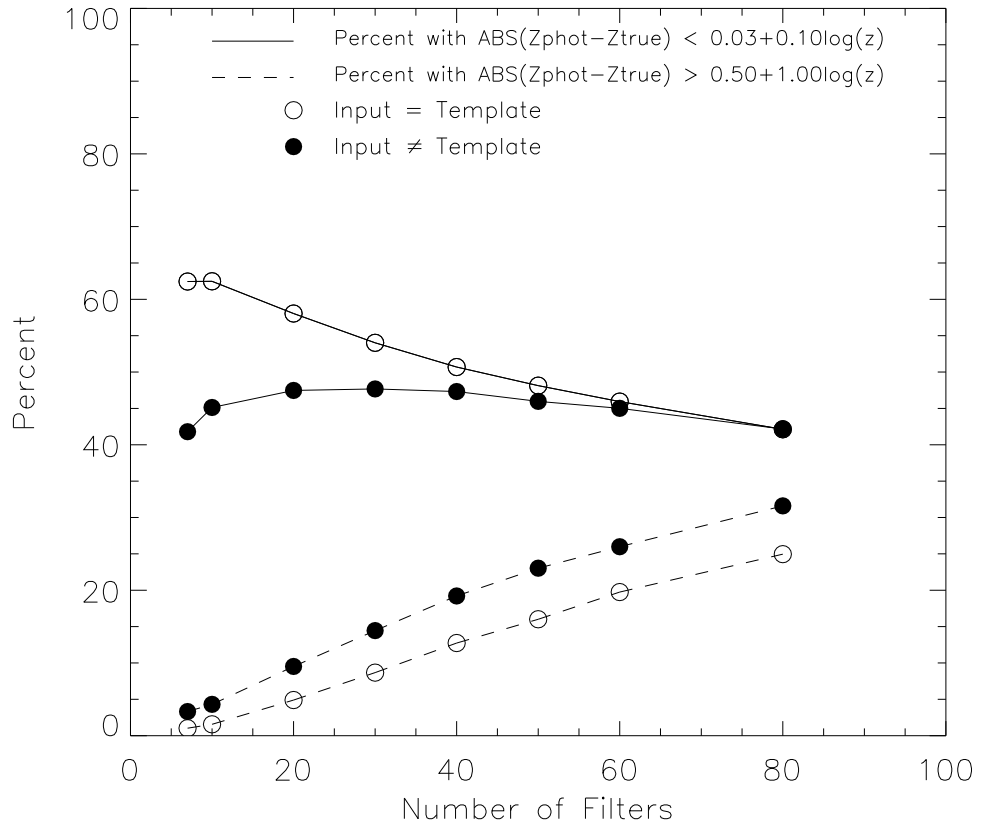


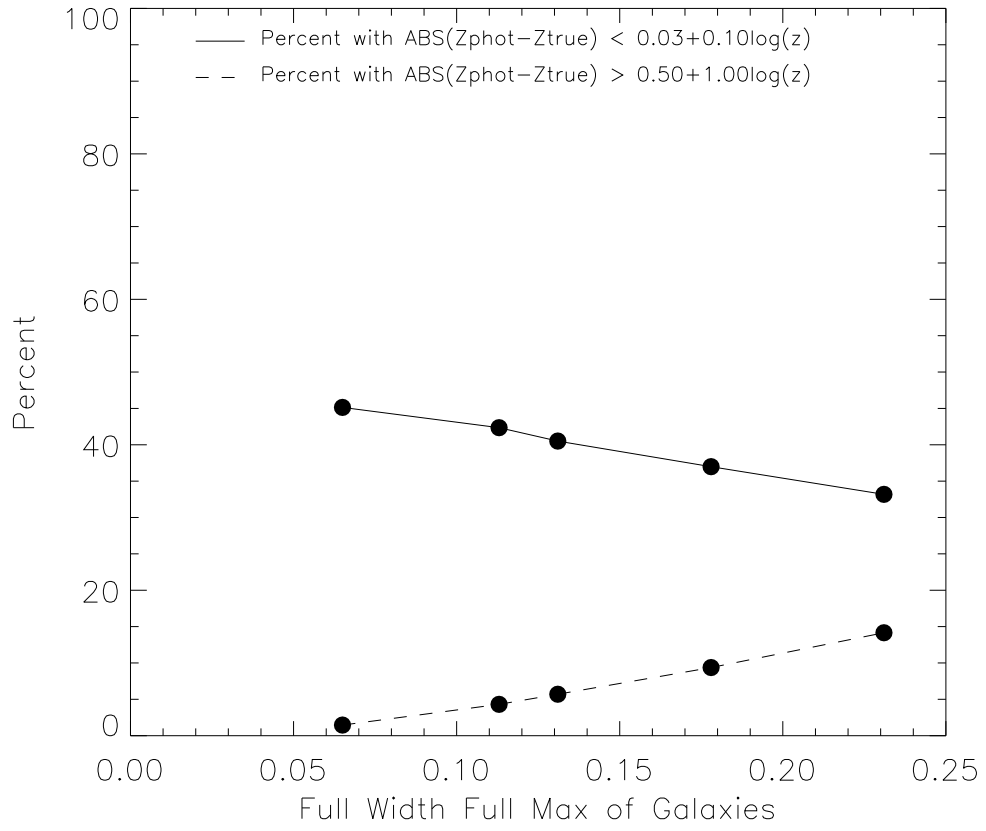














All Galaxies

